catalysts

MDPI

Article

Thermal Behavior of Heavy Oil Catalytic Pyrolysis and Aquathermolysis

Mohammed A. Khelkhal *, Semen E. Lapuk, Aleksey V. Buzyurov, Nikita E. Ignashev, Elvira I. Shmeleva, Irek I. Mukhamatdinov and Alexey V. Vakhin

Department of Petroleum Engineering, Kazan Federal University, Kremlevskaya Str. 18, 420008 Kazan, Russia; lapuksemen@gmail.com (S.E.L.); abuzurov95@gmail.com (A.V.B.); Ignashev13Nik@mail.ru (N.E.I.); El_Ga92@mail.ru (E.I.S.); imuhamatdinov@gmail.com (I.I.M.); vahin-a_v@mail.ru (A.V.V.)

* Correspondence: amine.khelkhal@gmail.com; Tel.: +7-(986)-916-39-12

Abstract: There is still considerable controversy surrounding the mechanisms, thermodynamics, and kinetics of heavy oil aquathermolysis and pyrolysis processes. The present paper aims to widen our knowledge about the effect of iron tallates on pyrolysis and aquathermolysis of Cuban heavy oil. The obtained SARA (S: saturates, A: aromatics, R: resins, A: asphaltenes) analysis has shown a significant increase in light hydrocarbon content during aquathermolysis. Moreover, the elemental analysis has indicated an increase in C and H content by almost 4% and 6%, respectively, with a significant decrease in S and O content by up to 23% in the presence of iron tallates. These results have been further confirmed by infrared spectrometry. The obtained IR data indicated that asphaltene and resin compounds transform into light hydrocarbons after aquathermolysis. On another hand, the activation energy of heavy oil pyrolysis decreased in the presence of the utilized catalyst; meanwhile, the reaction rate increased, especially in the temperature range of 200–480 °C, which may validate a significant effect of the used catalyst in real conditions. Moreover, the obtained thermodynamic data showed a decrease in the enthalpy and entropy of activation of oil pyrolysis in the presence of iron tallates. Our results are encouraging in terms of energy consumption, optimization, and process control and should be validated by a larger sample size.

Keywords: heavy oil; catalytic pyrolysis; iron tallates; aquathermolysis; kinetic models

Citation: Khelkhal, M.A.; Lapuk, S.E.; Buzyurov, A.V.; Ignashev, N.E.; Shmeleva, E.I.; Mukhamatdinov, I.I.; Vakhin, A.V. Thermal Behavior of Heavy Oil Catalytic Pyrolysis and Aquathermolysis. *Catalysts* **2022**, *12*, 449. https://doi.org/10.3390/catal12040449

Academic Editors: Hwai Chyuan Ong, Chia-Hung Su and Hoang Chinh Nguyen

Received: 10 March 2022
Accepted: 15 April 2022
Published: 18 April 2022

1. Introduction

Unconventional hydrocarbons are widely considered to be a potential alternative resource for satisfying energy demand associated with population growth and the shortage of conventional resources of energy such as light oil [1–4]. However, these hydrocarbons have been neglected due to the lack of efficient methods [5]. Heavy and extra-heavy oils are believed to be the most available source of energy on the planet [6–8]. These oils are characterized by a high viscosity which complicates the process of their extraction and processing. Nowadays, different types of methods, known as enhanced oil recovery methods, have been developed for the extraction of heavy and extra-heavy oil [9–14]. Among them, thermal methods still generate tremendous interest from experts due to their economic and environmental prospects [15].

It is common knowledge that thermal enhanced oil recovery methods are widely used to decrease the viscosity of heavy oil in situ. Moreover, these methods are able to increase significantly oil mobility toward producing wells. Perhaps, the main known methods widely used for heavy oil extraction nowadays are the processes of cyclic steam stimulation (CSS) [16] and steam-assisted gravity drainage (SAGD) [17,18]. Nevertheless, one of the major drawbacks of these processes is the low recovery factor and the high viscosity of produced oil which requires further processing and complicates transportation [19].

Within the next few years, catalyst application is likely to become an important component in the processes of steam injection [20] because catalytic agents can decrease

the activation energies of associated reactions and increase the rate at which they occur, as shown by several previous works [21,22]. To improve the process of steam injection, many experts [23–25] now argue that a deeper understanding of pyrolysis, aquathermolysis, and cracking reactions may be the main key, especially when it comes to the application of catalytic agents for this process.

Recently, a growing body of literature has investigated the effect of different catalysts on aquathermolysis and pyrolysis reactions [20,26,27]. In their works, Vakhin et al. [28–30] have studied the effect of different oil-soluble metal-based catalysts and found that Ni, Co, Fe, and Cu increase the saturate and aromatic contents in the oil after the steam effect.

It has been suggested that oil-soluble catalyst precursors transform during the steam injection processes and turn into nanoparticles able to break down the organosulfur compounds in asphaltenes by cleaving C-S bonds [19]. Unfortunately, most previous studies on oil aquathermolysis and pyrolysis reaction mechanisms neglected the kinetic and thermodynamic aspects of the process and did not focus on the energy's variation in the presence and absence of catalysts. The kinetic and thermodynamic parameters such as activation energy, enthalpy, and entropy are the main parameters that allow estimating the efficiency of the adopted catalyst.

This paper aims to validate the results obtained at larger laboratory scales regarding catalytic aquathermolysis and pyrolysis reactions in the presence of iron tallates from an analytical, non-isothermal kinetic, and thermodynamic point of view. In this context, we investigated the effect of iron tallates on oil composition during aquathermolysis and pyrolysis reactions. In addition, we calculated activation energies, enthalpy, and entropy of activation of the process of heavy oil pyrolysis by using a set of thermal analyses based on non-isothermal kinetics.

2. Experimental Section

2.1. Materials

In order to investigate the samples' composition and the kinetic and thermodynamic behavior of aquathermolysis and pyrolysis reactions, we have opted for a Cuban extra-heavy oil provided by JSC Zarubezhneft, Moscow, Russia from Boca de Jaruco's extra-heavy oil field. The physical properties of the used oil are described in Table 1. Organic solvents purer than 99.5% were obtained from Component Reactiv and utilized without additional purification. Inorganic salts were obtained from Sigma-Aldrich, Moscow, Russia. The physical characteristics of the used oil are presented in Table 1.

Table 1. Physical properties of Boca de Jaruco extra-heavy oil.

Physical Properties	Values
Oil density in reservoir conditions, kg/m^3	1029
Oil dynamic viscosity at 20 °C, mPa·s	271,000
Oil elemental composition, wt.%	
Carbon	75.47
Hydrogen	10.12
Oxygen	8.40
Sulfur	5.60
Nitrogen	0.41
Vanadium, nickel, iron	76, 26, 24

2.2. Catalyst Synthesis

The steps regarding iron tallate synthesis proceed very much in the same way as indicated in [31] with some modifications. Distilled tall oil (DTO) was chosen as a ligand-

forming agent for the precursor. Iron tallates have been obtained by mixing, firstly, 4 g of NaOH with 28.2 g of DTO at room temperature as follows:

$$C_{17}H_{33}COOH + NaOH \rightarrow C_{17}H_{33}COONa + H_2O$$

followed by reacting 30.4 g of the obtained carboxylates with 15.2 g of iron sulfate at higher temperatures (75–80 °C) as follows:

$$2C_{17}H_{33}COONa + FeSO_4 \rightarrow (C_{17}H_{33}COO)_2Fe + Na_2SO_4$$

The obtained iron tallates (61.8 g) have been used further for catalytic pyrolysis experiments.

2.3. Thermal Processing of the Extra-Heavy Oil and Its SARA and Elemental Analysis

To model the steam injection process of the extra-heavy oil thermal processing, we used a batch reactor equipped with a heated cylindrical thick-walled vessel made of steel, a thermocouple, an electric drive, and a manometer. The reactor temperature control was provided by a heating jacket and a cooling coil. The composition content of the initial oil has been obtained by SARA analysis. The obtained results are presented in Tables 2 and 3. It should be noted that the obtained oil from the thermal processing in the batch reactor is referred to as the control experiment throughout the text.

Table 2. SARA analysis of Boca de Jaruco extra-heavy oil.

Group Composition of Oil (SARA)	wt.%
Saturates	17.1
Aromatics	40.4
Resins	22.9
Asphaltenes	19.6

Table 3. Elemental analysis of the initial oil and its SARA fractions.

9		Elemental Analysis, wt.%				
		C	H	N	S	O
Initial oil	oil	75.47	10.12	0.41	5.60	8.40
	S	76.66	13.42	0.06	4.42	5.44
	A	83.31	11.03	0.09	2.34	3.23
	R	76.28	10.33	0.49	5.54	7.36
	A	74.39	8.57	0.87	6.30	9.87

2.4. Infrared Spectrometry Essays

So that we could study the structural group composition of the investigated products, we calculated the spectral coefficients. These coefficients define the ratio of the optical density values at the maxima of the corresponding absorption bands where $C_1 = D_{1600}/D_{720}$ (aromaticity), $C_2 = D_{1710}/D_{1465}$ (oxidation), $C_3 = D_{1380}/D_{1465}$ (branching), $C_4 = (D_{720} + D_{1380})/D_{1600}$ (aliphaticity), and $C_5 = D_{1030}/D_{1465}$ (saturation) using a baseline in the 2000–400 cm^{-1} spectrum. The first coefficient represents aromaticity which results from stretching vibrations of $C{=}C_{arom}$ bonds of aromatic rings. Next, the second coefficient (C_2) represents the oxidation which is associated with the presence of carbonyl groups (CO). Moreover, the third coefficient (C_3) is related to the structure of paraffin chains which can be estimated by their branching from CH_3/CH_2. The fourth factor is aliphaticity $(CH_3 + CH_2)/C = S_{arom}$, and it shows the proportion of methyl and methylene groups to aromatic groups; meanwhile, the fifth coefficient C_5 shows the proportion of sulfoxide groups.

2.5. Sample Preparation

So that we would be able to study the effect of iron tallates on extra-heavy oil pyrolysis reactions, we prepared a sample of pure extra-heavy oil and 2 wt.% of iron tallates in initial oil for thermal analysis.

2.6. Thermal Analysis

At a temperature range of 30–600 °C, differential scanning calorimetry (DSC) analysis was performed by using an STA 449 F1 Jupiter (Netzsch, Selb, Germany) thermoanalyzer at linear heating rates of 5, 10, 15, and 20 °C·min^{-1}, under 50 mL·min^{-1} flow of argon gas. Moreover, the mass of the studied samples was ~10 mg in the Al crucible. Data processing was performed using Proteus Analysis 5.2.1 and NETZSCH Kinetics Neo 2.1.2.2 program package.

Broadly speaking, steam-based processes are believed to include different reactions types such as pyrolysis [32,33] (thermolysis, thermal cracking), aquathermolysis, and gasification [34]. Moreover, these reactions are not widely understood in detail due to their complex nature and the heterogeneous mediums in which they occur. Therefore, determining the kinetic behavior of such reactions requires modern and sophisticated physical and chemical methods which may allow a detailed description of the processes associated with steam-based enhanced oil recovery methods. One of the most promising methods in the field of kinetics is the non-isothermal kinetic approach, which is consistent with the characteristics of such processes as steam injection. It is based on studying the aquathermolysis and pyrolysis reactions at different heating rates, unlike the conventional approach, which is based on studying different reactions at a constant temperature (isothermal principle), due to significant heat variations associated with these processes which lead to uncertain results.

2.7. Kinetic Theory

The process of extra-heavy oil pyrolysis is considered quite complicated for kinetic description, and it is often described as a function of conversion degree α, the preexponential factor A, and the apparent activation energy E_α in addition to the reaction model $f(\alpha)$ as follows:

$$\frac{d\alpha}{dt} = k(T)f(\alpha) = Aexp\left(-\frac{E_\alpha}{RT}\right)f(\alpha) \quad (1)$$

2.8. Isoconversional Kinetic Analysis

Thermal analysis in this study aims to determine the kinetic triplets of the processes occurring during steam-based methods of enhancing oil recovery. Therefore, we chose Kissinger–Akahira–Sunose (KAS) [35] and Friedman [36] methods as model-free analyses to obtain the energy of activation E_α and preexponential factor A of these processes.

The Kissinger–Akahir–Sunose (KAS) method is presented by the following equation:

$$\ln\left(-\frac{\beta_i}{T_{\alpha,i}{}^2}\right) = Const - \frac{E_\alpha}{RT_{\alpha,i}} \quad (2)$$

The Friedman method is described as follows:

$$\ln\left(\frac{d\alpha}{dt}\right)_{\alpha,i} = \ln[f(\alpha)A_\alpha] - \frac{E_\alpha}{RT_{\alpha,i}} \quad (3)$$

where the index i identifies an individual heating rate and $T_{\alpha,i}$ is the temperature at which the extent of conversion α is reached under ith heating rate. Then for any given α, the value of E_α is estimated from the slope of a plot of $\ln\left(\frac{d\alpha}{dt}\right)_{\alpha,i}$ against $\frac{1}{RT_{\alpha,i}}$ in the case of Friedman and from the slope of a plot of $\ln\left(-\frac{\beta_i}{T_{\alpha,i}{}^2}\right)$ against $\frac{1}{RT_{\alpha,i}}$ in the case of KAS. Next, for assuming the kinetic model and the reaction type, we proceeded to apply the model-based analysis

which depends mainly on the obtained values of activation energy, pre-exponential factor, reaction order, and rate. These models were optimized utilizing KineticsNeo software (Netzsch). Kinetic models have been performed with the lowest number of steps to obtain an acceptable fit and consistent approach with the pyrolysis process of Cuban extra-heavy oil. Table 4 presents the classical solid reaction kinetic description.

Table 4. Models' methods for calculating kinetic parameters.

Model	Equation
Reaction of nth order (Fn)	$f = (1 - \alpha)^n$
Two-dimensional phase boundary (R2)	$f = 2(1 - \alpha)^{1/2}$
Three-dimensional phase boundary (R3)	$f = 3(1 - \alpha)^{2/3}$
N-dimensional nucleation according to Avrami–Erofeev (An)	$f = n \cdot (1 - \alpha) \cdot [-\ln(1 - \alpha)]^{(n-1)/n}$
Expanded Prout–Tompkins equation (Bna)	$f = (1 - \alpha)^n \cdot \alpha^{AutocatOrder}$
The reaction of nth order with m-power autocatalysis by-product (Cnm)	$f = (1 - \alpha)^n \cdot (1 + AutocatOrder \cdot \alpha^m)$
Kamal–Sourur equation (KS)	$"Reaction\ rate = A" \cdot (1 - \alpha)^n \cdot [exp(-E/RT) + AutocatOrder \cdot \alpha^m \cdot exp(-E2/RT)]$

3. Discussion

3.1. Chemical Composition and Elemental Analysis

The results obtained from SARA analysis and elemental analysis of the initial heavy oil and oil after the batch reactor processing at higher temperature (250 °C) and pressure (90 atm) in the absence (control experiment) and the presence of iron tallates are presented in Figure 1 and Table 5, respectively.

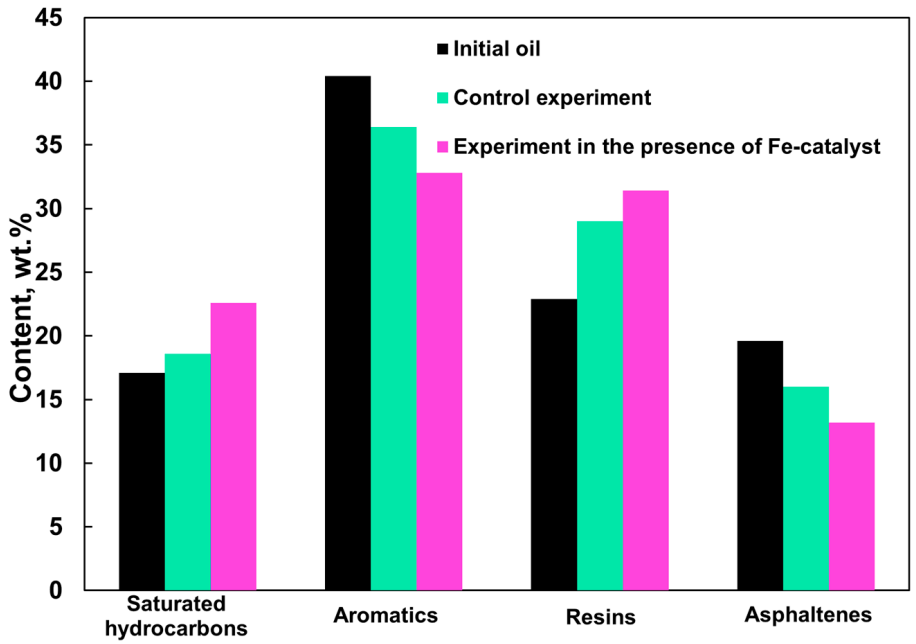

Figure 1. SARA analysis of the initial heavy oil and oil after the batch reactor processing at higher temperature (250 °C) and pressure (90 atm) in the absence (control experiment) and in the presence of iron tallates.

Table 5. Elemental analysis of catalytic and non-catalytic aquathermolysis products.

Sample		Elemental Analysis, wt.%				
		C	**H**	**N**	**S**	**O**
Non-catalytic steam thermal processing	oil	69.34	9.30	0.36	8.40	12.60
	S	79.17	13.92	0.06	2.74	4.11
	A	83.04	11.21	0.11	2.26	3.38
	R	76.48	10.69	0.55	4.91	7.37
	A	73.07	8.23	0.91	7.11	10.68
Catalytic steam thermal processing	oil	73.60	9.95	0.37	6.43	9.65
	S	80.92	14.04	0.06	2.09	2.89
	A	83.76	10.79	0.11	2.22	3.12
	R	67.09	9.29	0.38	9.76	13.48
	A	63.11	6.98	0.64	12.29	16.98

As seen in Figure 1, the quantity of saturated hydrocarbons in the presence of iron tallates is relatively higher than the amount found in the control experiment and even in the initial sample. This is probably due to the destruction of aromatic compounds which are in lower quantities in the catalytic process compared to the control and initial samples thermal treating. Moreover, Figure 1 shows a significant opposite relationship between asphaltene and resin content changes. In other words, the amount of asphaltenes in the catalytic experiments is less than the amount of asphaltenes in control and initial samples. Therefore, the increase in the amount of resins could be explained by the conversion of a part of asphaltene compounds into resin fractions.

On another hand, the elemental analysis of catalytic and non-catalytic aquathermolysis products (Table 5) indicates higher carbon and hydrogen amounts (73.60% and 9.95%) in the presence of iron tallates, unlike the non-catalytic process which showed low values for these elements (69.34% and 9.30% for carbon and hydrogen, respectively). The good effect of the used catalyst is expressed by the amounts of sulfur and oxygen as well, which decreased from 8.40% and 12.60%, respectively, in its presence to 6.43% and 9.65% in the non-catalytic process.

The same pattern has been established for the SARA elemental analysis which has indicated an increase in C amount in the saturates and aromatics in the presence of the catalyst compared to its absence as an indicator of C-C destruction reactions from aromatics into saturates. This could be confirmed by the amount of H in the saturates and aromatics, which decreased from 11.21% in the absence of the catalyst to 10.79% in its presence, and this is an indicator of hydrogen consumption during aromatic ring destruction in the presence of iron tallates.

The decrease in sulfur and oxygen amount in the presence of iron tallates is a result of catalyst precursor transformation into iron sulfide and iron oxygen molecules via thermal degradation at higher temperatures. The obtained iron sulfides and oxides probably present nanoparticle form and, in turn, play the role of the catalytic agent of the occurring reactions. There was a significant correlation between the elemental analysis of oil samples and their SARA fraction elemental data. Table 5 shows the significant increase in sulfur and oxygen content of the resin and asphaltene samples obtained in the presence of iron tallates, confirming our aforementioned hypotheses about the conversion of asphaltenes into resins which are found to enrich the amounts of the saturate and aromatic fractions; as a result, the heteroatoms would be present in greater quantities compared to carbon and hydrogen atoms.

So, to comprehend the composition change behavior and to support our findings, we have applied infrared spectrometry. The obtained results of the infrared spectrometry are presented in Table 6.

Table 6. Results of IR spectral analysis of oil samples.

No	Experimental Conditions			C_1	C_2	C_3	C_4	C_5
1	Initial oil			1.50	0.14	0.56	4.17	0.04
	Batch reactor experiments							
	Process	Pressure	T. °C	C_1	C_2	C_3	C_4	C_5
1	Control experiment	90	250	0.93	0.23	0.56	3.65	0.03
2	The experiment in the presence of iron tallates			1.13	0.22	0.68	3.62	0.10

According to the obtained results, we can observe the rise in aromaticity C_1 from 0.93 in the absence of the catalyst to 1.13 in its presence, which evidences the process of asphaltene destruction into aromatic-ring-containing resins. Moreover, it should be noted that in both thermal experiments, the aromaticity factor C_1 decreases, which also evidences the conversion of aromatic compounds into saturated hydrocarbons, as has been previously demonstrated by SARA and elemental analysis. Moreover, the increase in the oxidation factor C_2 indicates the occurrence of slight intermolecular oxidation processes leading to some oxygenated compounds contributing to improving the quality of the produced oil by forming some active catalytic agents such as iron oxide nanoparticles. On another hand, the obtained data show a significant increase in the branched aliphatic compounds as indicated by the branching factor C_3 values, which increase from 0.56 in the absence of catalyst for both the initial and the control experiment to 0.68 after the catalytic effect of iron tallates. This is in good agreement with elemental and SARA analysis, which suggests that the increase in saturated hydrocarbons is the result of the thermal cracking of the aromatic compounds within the oil composition. The aliphatic factor C_4 did not show a significant difference between the control experiment and the experiment conducted in the presence of iron tallates. On contrary, it decreased relative to the initial oil sample, which is expected because of the evaporation of light gases and hydrocarbons during the thermal processing. Finally, the saturation factor value is 3 times higher for the heavy oil catalytic process compared to those factors related to the initial and control experiment. This is a good indicator of the formation of sulfoxide groups in the presence of iron tallate catalysts, which enhance the catalytic processes of heavy oil pyrolysis, aquathermolysis, and cracking via the formation of iron sulfide nanoparticles at higher temperatures.

3.2. Kinetic Calculations

We opted for a small differential scanning calorimetry (DSC) sample size in the present study because this type of analysis is well known for better estimation of kinetic parameters [37,38] of extra-heavy oil pyrolysis process in the presence and absence of different catalysts.

So that we could compare the effect generated by the obtained catalyst on the process of extra-heavy oil pyrolysis, we utilized DSC. The DSC curves of the non-catalytic and catalytic pyrolysis are presented in Figure 2.

The obtained curves (endothermic peaks from 350 to 500 °C) indicate the pyrolysis zone. They show an adequate behavior for both catalytic and non-catalytic pyrolysis processes, which allowed us to implement kinetic calculations.

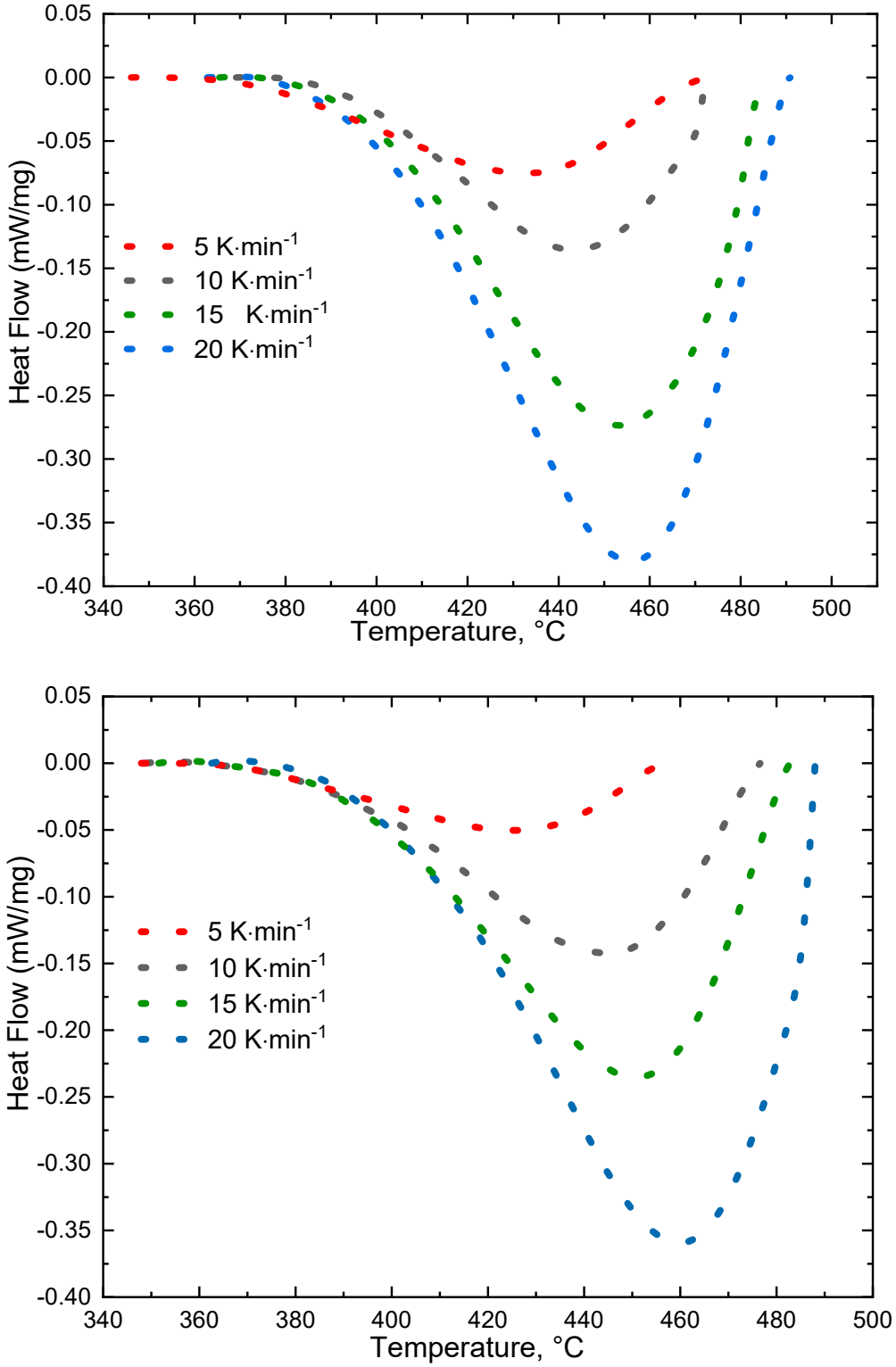

Figure 2. DSC curves for the process of extra-heavy oil pyrolysis in the absence (**Top**) and in the presence (**Bottom**) of iron tallates.

Table 7 contains the different values of activation energy and pre-exponential factor obtained during the pyrolysis processes in the presence and in the absence of iron tallates. In fact, the activation energies and the preexponential factors associated with Friedman, KAS, and ASTM E2890 values have been selected for a conversion degree of 0.5. These values are illustrated in Figure 3.

Table 7. Kinetic parameters of Cuban extra-heavy oil pyrolysis process obtained from the isoconversional methods for a conversion degree of 0.5.

Non-Catalytic Pyrolysis					
ASTM E2890		**ASTM E2890**		**ASTM E2890**	
$\mathbf{E_\alpha}$**, kJ·mol^{-1}**	$\mathbf{E_\alpha}$**, kJ·mol^{-1}**	$\mathbf{E_\alpha}$**, kJ·mol^{-1}**	$\mathbf{E_\alpha}$**, kJ·mol^{-1}**	$\mathbf{E_\alpha}$**, kJ·mol^{-1}**	$\mathbf{E_\alpha}$**, kJ·mol^{-1}**
224 ± 12	224 ± 12	224 ± 12	224 ± 12	224 ± 12	224 ± 12
Catalytic Pyrolysis					
ASTM E2890		**ASTM E2890**		**ASTM E2890**	
$\mathbf{E_\alpha}$**, kJ·mol^{-1}**	$\mathbf{E_\alpha}$**, kJ·mol^{-1}**	$\mathbf{E_\alpha}$**, kJ·mol^{-1}**	$\mathbf{E_\alpha}$**, kJ·mol^{-1}**	$\mathbf{E_\alpha}$**, kJ·mol^{-1}**	$\mathbf{E_\alpha}$**, kJ·mol^{-1}**
167 ± 14	167 ± 14	167 ± 14	167 ± 14	167 ± 14	167 ± 14

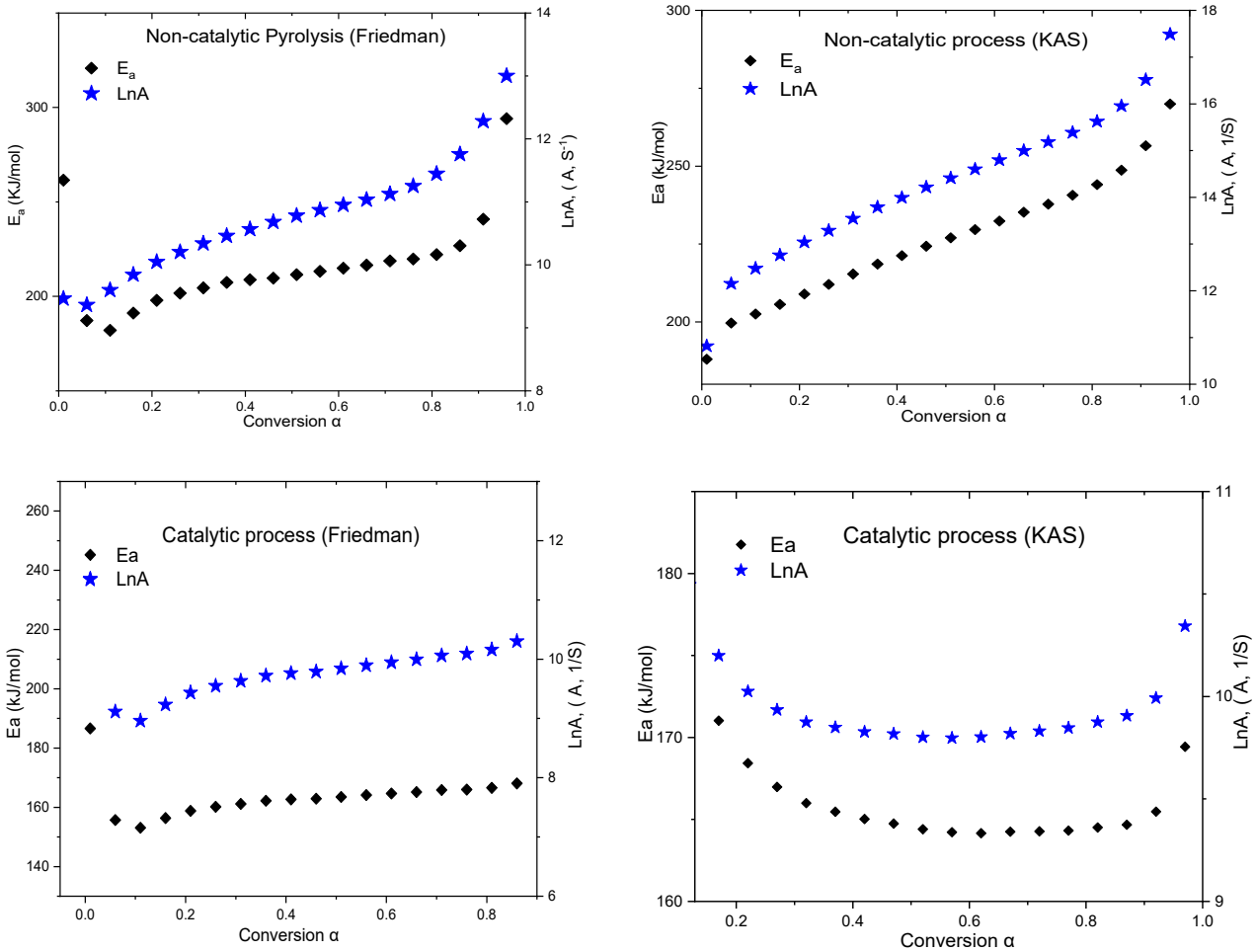

Figure 3. Pyrolysis activation energy dependency on conversion degree in the presence and absence of catalyst obtained by KAS and Friedman.

From the obtained data shown in Table 7 and Figure 3, we observe a decrease in activation energy in the presence of the catalyst, which reflects the efficiency of iron tallates as a pyrolysis catalyst. From another side, the curves of the non-catalytic pyrolysis demonstrate an increase in activation energies with conversion degree evolution. However, the catalytic pyrolysis demonstrates almost a constant value with conversion degree evolution, which is explained by the adopted autocatalytic mechanism of the process caused by the presence of iron tallates. The values of activation energy and preexponential factors in Table 8 confirm our hypothesis.

Table 8. Kinetic parameters of extra-heavy oil pyrolysis process obtained from the model-based methods.

Models	Pure Oil		Pure Oil with Catalyst	
	Kinetic Parameters	**R^2**	**Kinetic Parameters**	**R^2**
Fn	E = 215.8 kJ·mol^{-1} lnA = 13.7 ReactOrder n = 1.1	0.99175	E= 175.6 kJ·mol^{-1} lnA = 10.6 ReactOrder n = 0.8	0.99473
R2	E = 147.4 kJ·mol^{-1} lnA = 8.2	0.96275	E = 141.5 kJ·mol^{-1} lnA = 7.8	0.98479
R3	E = 167.3 kJ·mol^{-1} lnA = 9.5	0.98117	E = 161.1 kJ·mol^{-1} lnA = 9	0.99321
An	E = 273.4 kJ·mol^{-1} lnA = 17.9 Dimension n = 0.8	0.99359	E = 161 lnA = 9.6 Dimension n = 1.2	0.99517
Bna	E = 213.5 kJ·mol^{-1} lnA = 13.5 ReactOrder n = 1.1 AutocatOrder 0.01	0.99160	E = 156.4 lnA = 9.3 ReactOrder n = 0.8 AutocatOrder 0.14	0.99559
Cnm	E = 222.3 kJ·mol^{-1} lnA = 13.8 ReactOrder n = 1.2 AutocatOrder 0.01 AutocatPower m = 0.01	0.99153	E = 155.5 lnA = 5 ReactOrder n = 0.8 AutocatOrder 4.3 AutocatPower m = 0.15	0.99558
KS	E = 604.3 kJ·mol^{-1} E2 = 227.3 kJ·mol^{-1} lnA = 11 ReactOrder n = 1.2 AutocatOrder 3.5 AutocatPower m = 0.01	0.99109	E = 647 E2 = 163 lnA = 9.7 ReactOrder n = 0.9 AutocatOrder 0.02 AutocatPower m = 0.1	0.99536

The obtained values of activation energy and preexponential factors obtained from model-based methods demonstrate a similar approach in terms of increasing the energy of activation of the oil pyrolysis process in the presence of iron tallates for all models except the KS model. Broadly speaking, the parameters obtained using the isoconversional approach should coincide with the parameters obtained using the model method as recommended by International Confederation for Thermal Analysis and Calorimetry (ICTAC). Based on this recommendation and taking into account the correlation coefficients, it has been found that the corresponding reaction models and isoconversional methods that adequately describe the process of Cuban extra-heavy oil pyrolysis are the Bna and Cnm models, as well as the Friedman isoconversional method in addition to ASTM E2890.

The next figure (Figure 4) demonstrates the correlation between experimental DSC curves obtained for the extra-heavy oil pyrolysis process and the fit DSC curves for this process based on a model corresponding to n-order autocatalysis reaction with m-power by-product (Cnm) in the presence and the absence of iron tallates.

Interestingly, the obtained results have shed light on the nature of the process of Cuban extra-heavy oil pyrolysis in the presence and the absence of iron tallates. It is worth noting that the obtained Cnm model provides the same results regarding activation energy decreasing in the presence of iron tallates. Moreover, according to the Cnm model, the process of Cuban extra-heavy oil pyrolysis could be described by a set of autocatalytic reactions. In addition, the parameters related to these autocatalytic reactions are well improved by the presence of iron tallates, where the autocatalytic reaction order is greater (4.3) in the presence of iron tallates compared to the non-catalytic pyrolysis (0.01). Besides, autocatalytic reaction parameter m-power increases to 0.15 in the presence of iron tallates compared to when pyrolysis occurs without any catalyst (0.01).

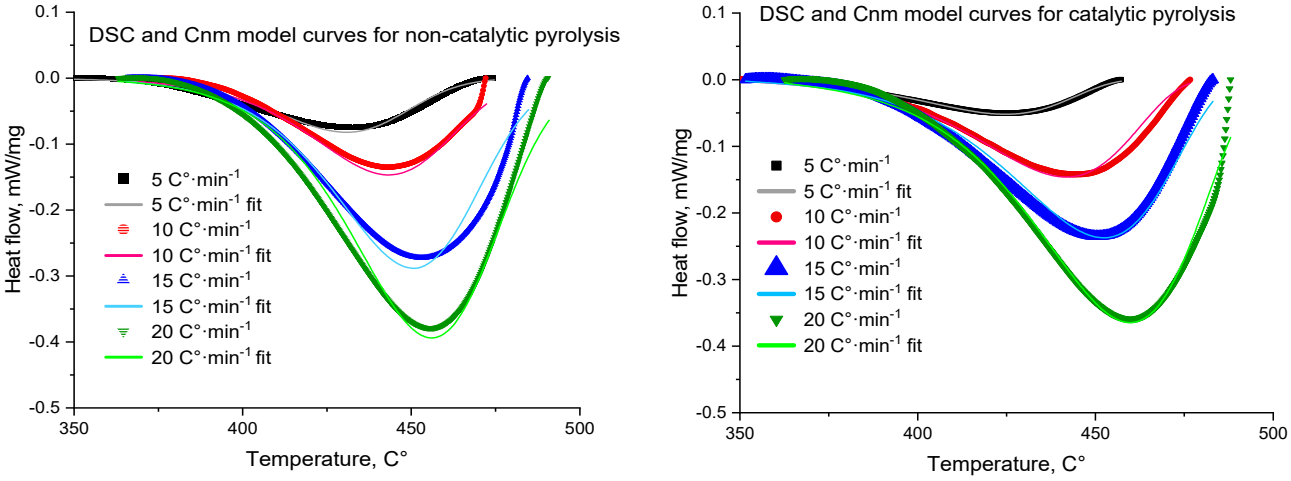

Figure 4. Correlation between experimental DSC curves obtained for extra-heavy oil pyrolysis process and the fit DSC curves for this process based on a model corresponding to n-order autocatalysis reaction with m-power by-product (Cnm) in the presence and the absence of iron tallates.

Regardless of the good effect highlighted by the values of activation energy, autocatalytic order, and power, we have noted that the preexponential factors, however, demonstrate a decrease in values in the presence of iron tallates for all isoconversional and model-based methods. Therefore, to confirm our hypothesis about the efficiency of iron tallates in the process of Cuban extra-heavy oil pyrolysis we calculated the half-life times of the pyrolysis processes in the presence and absence of the catalyst to predict the associated reactions rates, as shown in Figure 5, at a temperature range of 200 °C to 400 °C, which is believed the range at which oil pyrolysis occurs.

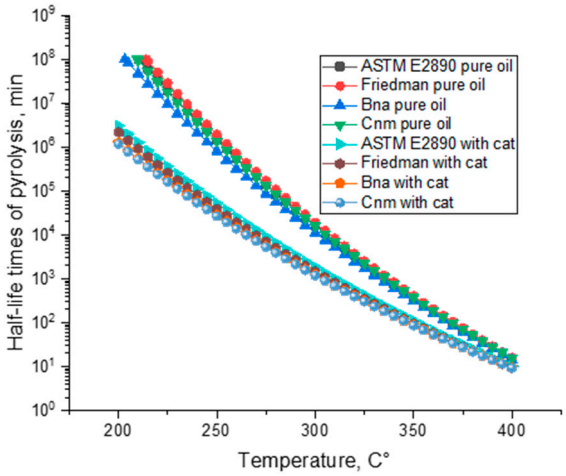

Figure 5. The calculated pyrolysis half-life times from model and non-model approaches at a temperature range of 200 °C to 400 °C in the presence and absence of the catalyst.

The obtained half-life times demonstrate higher pyrolysis reaction rates in the presence of iron tallates, especially at lower temperatures (less than 300 °C), which are believed to be the most intense zone of oil pyrolysis processes. Our results are consistent with previous works on heavy oil pyrolysis at larger scales [28–30] and our conclusions suggest the same hypothesis about C-S bonds breaking at a temperature less than 300 °C, transforming higher oil components into light fractions and therefore enhancing oil quality and decreasing oil viscosity.

3.3. Thermodynamic Functions of Activated Complex Formation

To calculate thermodynamic parameters of activated complex formation, we have used the Eyring equation:

$$k(T) = \frac{K_B T}{h} exp\left(-\frac{\Delta^{\ddagger} G^0}{RT}\right) \quad (4)$$

where K_B and h are the Boltzmann and Planck constants and $\Delta^{\ddagger}G^0$ is the standard Gibbs energy of activation complex formation.

The sophisticated Eyring equation is useful for giving insight into the nature of any transition state. In fact, the following equations could be useful for relating the thermodynamic and kinetic parameters obtained by the Arrhenius equation if we consider pyrolysis as a one-step process at each conversion degree:

$$\Delta^{\ddagger} H^0 = E_\alpha - RT_{st} \quad (5)$$

$$\Delta^{\ddagger} S^0 = R\left(ln\frac{hA_\alpha}{K_B T_{st}} - 1\right) \quad (6)$$

$$\Delta^{\ddagger} G^0 = \Delta^{\ddagger} H^0 - T_{st}\Delta^{\ddagger} S^0 \quad (7)$$

where $\Delta^{\ddagger}H^0$ and $\Delta^{\ddagger}S^0$ are standard enthalpy and entropy of activation complex formation, and T_{st} is a standard temperature which was defined as the peak temperature at the minimum heating rate (716 K). According to Equations (5) and (6), the activation energy is related to the energy difference between reactants and the transition state, and the pre-exponential factor is related to the change in order degree.

To calculate the thermodynamic functions, the Arrhenius parameters derived from KAS and Friedman methods were used. The calculated results are presented in Table 9.

Table 9. Thermodynamic parameters for catalytic and non-catalytic pyrolysis processes based on KAS and Friedman methods.

	Pure Oil			**Oil with Catalyst**		
α (%)	$\frac{\Delta^{\ddagger}H^0}{\mathbf{kJ \cdot mol^{-1}}}$	$\frac{\Delta^{\ddagger}S^0}{\mathbf{J \cdot mol^{-1} \cdot K^{-1}}}$	$\frac{\Delta^{\ddagger}G^0}{\mathbf{kJ \cdot mol^{-1}}}$	$\frac{\Delta^{\ddagger}H^0}{\mathbf{kJ \cdot mol^{-1}}}$	$\frac{\Delta^{\ddagger}S^0}{\mathbf{J \cdot mol^{-1} \cdot K^{-1}}}$	$\frac{\Delta^{\ddagger}G^0}{\mathbf{kJ \cdot mol^{-1}}}$
			Friedman method			
10	196 ± 25	−19 ± 4	209 ± 25	147 ± 19	−90 ± 3	211 ± 19
20	211 ± 21	3 ± 4	209 ± 21	153 ± 16	−80.5 ± 2.8	210 ± 16
30	221 ± 18	17 ± 3	209 ± 18	155 ± 14	−76.4 ± 2.5	210 ± 14
40	229 ± 18	27 ± 3	209 ± 18	157 ± 15	−73.6 ± 2.5	210 ± 15
50	236 ± 19	37 ± 3	209 ± 19	158 ± 15	−72.3 ± 2.6	209 ± 16
60	242 ± 21	44 ± 3	210 ± 21	159 ± 16	−70.3 ± 2.7	209 ± 16
70	248 ± 22	52 ± 4	210 ± 22	160 ± 16	−68.4 ± 2.7	209 ± 17
80	257 ± 23	65 ± 4	211 ± 24	161 ± 17	−66.3 ± 2.8	208 ± 17
90	283 ± 31	99 ± 5	211 ± 31	167 ± 18	−55.2 ± 2.9	207 ± 18
Aver	236	36	209	157	−72.6	209
			KAS method			
10	196 ± 44	−23 ± 8	212 ± 45	173 ± 14	−54.2 ± 2.4	212 ± 14
20	202 ± 35	−12 ± 6	211 ± 35	163 ± 13	−67.5 ± 2.3	212 ± 14
30	209 ± 30	−2 ± 5	210 ± 30	160 ± 14	−71.1 ± 2.3	211 ± 14
40	215 ± 26	7 ± 4	210 ± 26	159 ± 14	−72.2 ± 2.3	211 ± 14

Table 9. *Cont.*

	Pure Oil			Oil with Catalyst		
α (%)	$\frac{\Delta^{\ddagger}H^0}{\mathbf{kJ \cdot mol^{-1}}}$	$\frac{\Delta^{\ddagger}S^0}{\mathbf{J \cdot mol^{-1} \cdot K^{-1}}}$	$\frac{\Delta^{\ddagger}G^0}{\mathbf{kJ \cdot mol^{-1}}}$	$\frac{\Delta^{\ddagger}H^0}{\mathbf{kJ \cdot mol^{-1}}}$	$\frac{\Delta^{\ddagger}S^0}{\mathbf{J \cdot mol^{-1} \cdot K^{-1}}}$	$\frac{\Delta^{\ddagger}G^0}{\mathbf{kJ \cdot mol^{-1}}}$
50	220 ± 23	15 ± 4	210 ± 23	159 ± 14	−72.8 ± 2.3	211 ± 14
60	226 ± 21	22 ± 4	210 ± 22	158 ± 14	−72.9 ± 2.4	211 ± 14
70	231 ± 20	29 ± 3	210 ± 21	158 ± 15	−72.4 ± 2.5	210 ± 15
80	237 ± 21	38 ± 3	210 ± 21	159 ± 15	−71.7 ± 2.5	210 ± 15
90	249 ± 20	53 ± 3	211 ± 21	159 ± 16	−70.1 ± 2.6	209 ± 16
Aver	221	14	210	161	−69.4	211

From Table 9, we can see that thermodynamic functions calculated based on Arrhenius parameters derived from the KAS and Friedman methods converge well with each other within uncertainties. Comparison of the activation enthalpies for the process in the presence and absence of the catalyst indicates that the use of iron tallates significantly reduces the energy consumption for the formation of an activated complex and also makes it possible to avoid a significant increase in the activation enthalpy as pyrolysis proceeds. However, at the same time, when using the catalyst, the activation entropy is significantly reduced, which indicates a greater degree of arrangement of the transition state. Therefore, at high temperatures, the beneficial decrease in enthalpy will be largely suppressed by the entropy contribution ($\Delta^{\ddagger}G^0$ is about the same for both processes). At the same time, at lower temperatures, the entropy contribution will be much smaller, so the process in the presence of iron tallates will proceed much faster (see Figure 5).

4. Conclusions

Taken together, the results of the present study have shed light on the kinetic behavior of Cuban oil pyrolysis in the presence and absence of iron tallates. During this study, iron tallates were obtained and used as a material of investigation alongside oil samples. We applied thermal analysis to study the kinetic behavior of oil under different heating rates. The obtained SARA analysis has shown a significant increase in the content of light hydrocarbons (saturates and aromatics) during the oil catalytic aquathermolysis reactions. Moreover, the elemental analysis has indicated an increase in C and H content by almost 4% and 6%, respectively, with a significant decrease in S and O content by up to 23% in the presence of iron tallates. These results have been further confirmed by infrared spectrometry, which evidenced the conversion of asphaltene and resin fractions into light hydrocarbons. Moreover, our results have indicated a significant decrease in activation energy in the presence of iron tallates. Moreover, our hypothesis about catalyst efficiency has been confirmed further by predicting the pyrolysis reaction rate in the presence and absence of iron tallates via calculating pyrolysis half-life times at 200 °C to 400 °C and finding that iron tallates increase the pyrolysis process rate in a significant manner, especially at lower temperatures, which are supposed to be the temperatures of pyrolysis initiation and evolution. In addition, the evidence from this study suggests that the process of Cuban extra-heavy oil pyrolysis includes reactions of n^{th} order with m-power autocatalysis by-product. The evidence from the thermodynamic study suggests that the adopted catalyst for the process of Cuban extra-heavy oil pyrolysis reduces the enthalpy and entropy of activation, which may be useful for energy consumption optimization and process control. We believe that these findings add to a growing body of literature on extra-heavy oil upgrading technologies via thermal enhanced oil recovery methods. The obtained results are encouraging and may improve the application of steam injection processes, especially in the presence of oil-soluble catalysts.

Author Contributions: M.A.K.: formal analysis, investigation, writing—original draft, visualization, conceptualization. S.E.L.: formal analysis, data curation, visualization. A.V.B.: formal analysis, investigation. N.E.I.: formal analysis, investigation. E.I.S.: formal analysis, investigation. I.I.M.: formal analysis, investigation. A.V.V.: formal analysis, investigation, visualization, funding acquisition. All authors discussed and approved the final version. All authors have read and agreed to the published version of the manuscript.

Funding: This research received no external funding.

Acknowledgments: This work was supported by the Russian Science Foundation (grant No. 21-73-30023).

Conflicts of Interest: The authors declare that there is no conflict of interest regarding the publication of this paper.

References

1. Ahmed, U.; Meehan, D.N. *Unconventional Oil and Gas Resources: Exploitation and Development*; CRC Press: Boca Raton, FL, USA, 2019; ISBN 1498759416.
2. Kryukov, V.; Moe, A. Does Russian unconventional oil have a future? *Energy Policy* **2018**, *119*, 41–50. [CrossRef]
3. Wang, J.; Feng, L.; Steve, M.; Tang, X.; Gail, T.E.; Mikael, H. China's unconventional oil: A review of its resources and outlook for long-term production. *Energy* **2015**, *82*, 31–42. [CrossRef]
4. Castro-Alvarez, F.; Marsters, P.; de León Barido, D.P.; Kammen, D.M. Sustainability lessons from shale development in the United States for Mexico and other emerging unconventional oil and gas developers. *Renew. Sustain. Energy Rev.* **2018**, *82*, 1320–1332. [CrossRef]
5. Kapustin, N.O.; Grushevenko, D.A. Global prospects of unconventional oil in the turbulent market: A long term outlook to 2040. *Oil Gas Sci. Technol. IFP Energies Nouv.* **2018**, *73*, 67. [CrossRef]
6. Vakhin, A.V.; Khelkhal, M.A.; Tajik, A.; Ignashev, N.E.; Krapivnitskaya, T.O.; Peskov, N.Y.; Glyavin, M.Y.; Bulanova, S.A.; Slavkina, O.V.; Schekoldin, K.A. Microwave Radiation Impact on Heavy Oil Upgrading from Carbonate Deposits in the Presence of Nano-Sized Magnetite. *Processes* **2021**, *9*, 2021. [CrossRef]
7. Meyer, R.F.; Attanasi, E.D.; Freeman, P.A. *Heavy Oil and Natural Bitumen Resources in Geological Basins of the World: Map Showing Klemme Basin Classification of Sedimentary Provinces Reporting Heavy Oil or Natural Bitumen*; U.S. Geological Survey Open-File Report; U.S. Geological Survey: Reston, VA, USA, 2007; Volume 2007, p. 1084.
8. Guo, K.; Li, H.; Yu, Z. In-situ heavy and extra-heavy oil recovery: A review. *Fuel* **2016**, *185*, 886–902. [CrossRef]
9. Alvarado, V.; Manrique, E. Enhanced oil recovery: An update review. *Energies* **2010**, *3*, 1529–1575. [CrossRef]
10. Mokheimer, E.M.A.; Hamdy, M.; Abubakar, Z.; Shakeel, M.R.; Habib, M.A.; Mahmoud, M. A comprehensive review of thermal enhanced oil recovery: Techniques evaluation. *J. Energy Resour. Technol.* **2019**, *141*, 30801. [CrossRef]
11. Elbaz, A.M.; Gani, A.; Hourani, N.; Emwas, A.-H.; Sarathy, S.M.; Roberts, W.L. TG/DTG, FT-ICR mass spectrometry, and NMR spectroscopy study of heavy fuel oil. *Energy Fuels* **2015**, *29*, 7825–7835. [CrossRef]
12. Jameel, A.G.A.; Khateeb, A.; Elbaz, A.M.; Emwas, A.-H.; Zhang, W.; Roberts, W.L.; Sarathy, S.M. Characterization of deasphalted heavy fuel oil using APPI (+) FT-ICR mass spectrometry and NMR spectroscopy. *Fuel* **2019**, *253*, 950–963. [CrossRef]
13. Elbaz, A.M.; Roberts, W.L. PM from the combustion of heavy fuel oils. *Energy* **2018**, *152*, 455–465. [CrossRef]
14. Vakhin, A.V.; Khelkhal, M.A.; Tajik, A.; Gafurov, M.R.; Morozov, O.G.; Nasybullin, A.R.; Karandashov, S.A.; Ponomarev, A.A.; Krapivnitskaia, T.O.; Glyavin, M.Y. The Role of Nanodispersed Catalysts in Microwave Application during the Development of Unconventional Hydrocarbon Reserves: A Review of Potential Applications. *Processes* **2021**, *9*, 420. [CrossRef]
15. Kovscek, A.R. Emerging challenges and potential futures for thermally enhanced oil recovery. *J. Pet. Sci. Eng.* **2012**, *98*, 130–143. [CrossRef]
16. Kamari, A.; Nikookar, M.; Mohammadi, A.H. Study of the Performance of Cyclic Steam Stimulation (CSS) Oil Recovery Method in a Naturally-Fractured Carbonate Reservoir. In *Enhanced Oil Recovery: Methods, Economic Benefits and Impacts on the Environment*; Nova Science Publishers, Inc.: Hauppauge, NY, USA, 2015.
17. Mukhamatdinov, I.I.; Salih, I.S.S.; Khelkhal, M.A.; Vakhin, A.V. Application of Aromatic and Industrial Solvents for Enhancing Heavy Oil Recovery from the Ashalcha Field. *Energy Fuels* **2020**, *35*, 374–385. [CrossRef]
18. Shen, C. SAGD for heavy oil recovery. In *Enhanced Oil Recovery Field Case Studies*; Elsevier: Amsterdam, The Netherlands, 2013; pp. 413–445.
19. Hamedi Shokrlu, Y. Enhancement of Heavy Oil/Bitumen Thermal Recovery Using Nano Metal Particles. Ph.D. Thesis, University of Alberta, Edmonton, AB, Canada, 2014.
20. Ghashghaee, M.; Shirvani, S.; Kegnæs, S. Steam catalytic cracking of fuel oil over a novel composite nanocatalyst: Characterization, kinetics and comparative perspective. *J. Anal. Appl. Pyrolysis* **2019**, *138*, 281–293. [CrossRef]
21. Farhadian, A.; Khelkhal, M.A.; Tajik, A.; Lapuk, S.E.; Rezaeisadat, M.; Eskin, A.A.; Rodionov, N.O.; Vakhin, A.V. Effect of Ligand Structure on the Kinetics of Heavy Oil Oxidation: Toward Biobased Oil-Soluble Catalytic Systems for Enhanced Oil Recovery. *Ind. Eng. Chem. Res.* **2021**, *60*, 14713–14727. [CrossRef]

22. Khelkhal, M.A.; Eskin, A.A.; Nurgaliev, D.K.; Vakhin, A.V. Thermal study on stabilizing combustion front via bimetallic Mn@Cu tallates during heavy oil oxidation. *Energy Fuels* **2019**, *34*, 5121–5127. [CrossRef]
23. Jameel, A.G.A.; Han, Y.; Brignoli, O.; Telalović, S.; Elbaz, A.M.; Im, H.G.; Roberts, W.L.; Sarathy, S.M. Heavy fuel oil pyrolysis and combustion: Kinetics and evolved gases investigated by TGA-FTIR. *J. Anal. Appl. Pyrolysis* **2017**, *127*, 183–195. [CrossRef]
24. Amer, M.W.; Alhesan, J.S.A.; Marshall, M.; Awwad, A.M.; Al-Ayed, O.S. Characterization of Jordanian oil shale and variation in oil properties with pyrolysis temperature. *J. Anal. Appl. Pyrolysis* **2019**, *140*, 219–226. [CrossRef]
25. Al-Absi, A.A.; Aitani, A.M.; Al-Khattaf, S.S. Thermal and catalytic cracking of whole crude oils at high severity. *J. Anal. Appl. Pyrolysis* **2020**, *145*, 104705. [CrossRef]
26. Sitnov, S.; Mukhamatdinov, I.; Aliev, F.; Khelkhal, M.A.; Slavkina, O.; Bugaev, K. Heavy oil aquathermolysis in the presence of rock-forming minerals and iron oxide (II, III) nanoparticles. *Pet. Sci. Technol.* **2020**, *38*, 574–579. [CrossRef]
27. Faillace, J.G.; de Melo, C.F.; de Souza, S.P.L.; da Costa Marques, M.R. Production of light hydrocarbons from pyrolysis of heavy gas oil and high density polyethylene using pillared clays as catalysts. *J. Anal. Appl. Pyrolysis* **2017**, *126*, 70–76. [CrossRef]
28. Vakhin, A.V.; Aliev, F.A.; Mukhamatdinov, I.I.; Sitnov, S.A.; Sharifullin, A.V.; Kudryashov, S.I.; Afanasiev, I.S.; Petrashov, O.V.; Nurgaliev, D.K. Catalytic aquathermolysis of boca de jaruco heavy oil with nickel-based oil-soluble catalyst. *Processes* **2020**, *8*, 532. [CrossRef]
29. Vakhin, A.V.; Mukhamatdinov, I.I.; Aliev, F.A.; Kudryashov, S.I.; Afanasiev, I.S.; Petrashov, O.V.; Sitnov, S.A.; Chemodanov, A.E.; Varfolomeev, M.A.; Nurgaliev, D.K. Aquathermolysis of heavy oil in reservoir conditions with the use of oil-soluble catalysts: Part II–changes in composition of aromatic hydrocarbons. *Pet. Sci. Technol.* **2018**, *36*, 1850–1856. [CrossRef]
30. Vakhin, A.V.; Aliev, F.A.; Kudryashov, S.I.; Afanasiev, I.S.; Petrashov, O.V.; Sitnov, S.A.; Mukhamatdinov, I.I.; Varfolomeev, M.A.; Nurgaliev, D.K. Aquathermolysis of heavy oil in reservoir conditions with the use of oil-soluble catalysts: Part I–changes in composition of saturated hydrocarbons. *Pet. Sci. Technol.* **2018**, *36*, 1829–1836. [CrossRef]
31. Feoktistov, D.A.; Kayukova, G.P.; Vakhin, A.V.; Sitnov, S.A. Catalytic Aquathermolysis of High-Viscosity Oil Using Iron, Cobalt, and Copper Tallates. *Chem. Technol. Fuels Oils* **2018**, *53*, 905–912. [CrossRef]
32. Li, J.; Tang, X.; Chen, X.; Zhang, M.; Zheng, X.; Wang, C.; Deng, C. Viscosity reduction process of heavy oil by catalytic co-pyrolysis with sawdust. *J. Anal. Appl. Pyrolysis* **2019**, *140*, 444–451. [CrossRef]
33. Guo, W.; Yang, Q.; Sun, Y.; Xu, S.; Kang, S.; Lai, C.; Guo, M. Characteristics of low temperature co-current oxidizing pyrolysis of Huadian oil shale. *J. Anal. Appl. Pyrolysis* **2020**, *146*, 104759. [CrossRef]
34. Kapadia, P.R.; Kallos, M.S.; Gates, I.D. A comprehensive kinetic theory to model thermolysis, aquathermolysis, gasification, combustion, and oxidation of Athabasca bitumen. In Proceedings of the SPE Improved Oil Recovery Symposium, Tulsa, OK, USA, 25–29 April 2010; OnePetro: Richardson, TX, USA, 2010.
35. Vyazovkin, S. *Isoconversional Kinetics of Thermally Stimulated Processes*; Springer: Berlin, Germany, 2015; ISBN 9783319141756.
36. Friedman, H.L. Kinetics of thermal degradation of char-forming plastics from thermogravimetry. Application to a phenolic plastic. *J. Polym. Sci. Part C Polym. Symp.* **1964**, *6*, 183–195. [CrossRef]
37. Kok, M.V.; Gundogar, A.S. DSC study on combustion and pyrolysis behaviors of Turkish crude oils. *Fuel Process. Technol.* **2013**, *116*, 110–115. [CrossRef]
38. Varfolomeev, M.A.; Rakipov, I.T.; Isakov, D.R.; Nurgaliev, D.K.; Kok, M.V. Characterization and kinetics of siberian and tatarstan regions crude oils using differential scanning calorimetry. *Pet. Sci. Technol.* **2015**, *33*, 865–871. [CrossRef]